Journal of
MATERIALS RESEARCH

The influence of crystallization route on the $SrBi_2Nb_2O_9$ thin films

S. M. Zanetti, E. R. Leite, and E. Longo
Departamento de Química, UFSCar, P.O. Box 676, 13560-905 São Carlos, SP, Brazil

J. A. Varela
Instituto de Química, UNESP, P.O. Box 355, 14801-970 Araraquara, SP, Brazil

(Received 29 January 1998; accepted 6 August 1998)

Polycrystalline $SrBi_2Nb_2O_9$-layered ferroelectric thin films were synthesized on $Pt/Ti/SiO_2/Si$ substrate using the polymeric precursors solution. The dip-coated films were specular and crack-free and crystallized during firing at 700 °C. Single-, double-, and triple-layered films were obtained by several dips in the deposition solution, and the influence of crystallization between each dip was studied. Microstructure and morphological evaluation were followed by grazing incident x-ray diffraction (GIXRD), scanning electron microscopy (SEM), and atomic force microscopy (AFM). Multilayered films obtained using the intermediate-crystallized layer route present a dense microstructure with spherical grains, with a preferential orientation in the ⟨215⟩ direction; films obtained using the intermediate-amorphous layer route are polycrystalline and present elongated grains around 250 nm in size.

I. INTRODUCTION

The bismuth-based, layer-structured perovskites include a broad family of structural forms $(A_{m-1}B_mO_{3m+1})^{2+}(Bi_2O_2)^{2-}$, e.g., $SrBi_4Ti_4O_{15}$ (SBIT), $SrBi_2Ta_2O_9$ (SBT), and $SrBi_2Nb_2O_9$ (SBN). These kinds of materials have attracted much attention due to the possibility of applications such as nonvolatile memory devices. Nonvolatile memory is an application which truly utilizes the ferroelectric nature of the films and has potentially great practical impact. $Pb(Zr, Ti)O_3$ (PZT) has been widely studied for application to nonvolatile memory devices. However, PZT films on Pt electrodes present serious problems of degradation due to oxygen vacancies created at the interface. In addition, PZT capacitors do not maintain good electrical properties when PZT layer is <100 nm. Recent studies have reported that these bismuth-layered materials have presented good ferroelectric properties.[1,2]

Several preparation methods of Bi-layer thin films such as laser ablation,[1,3,4] sputtering,[5] metalorganic chemical vapor deposition (MOCVD),[6–8] sol-gel,[9,10] and metalorganic decomposition,[11–13] have been employed. Normally, physical methods have the disadvantage of requiring sophisticated and expensive equipment. Although the sol-gel method is considered very good in terms of stoichiometric control and introduction of dopants, it presents a serious problem of solution aging. The aging may alter the film microstructure, causing significant ferroelectric loss.[14]

Recently, a new approach for thin film chemical synthesis, based on the process developed by Pechini,[15] has been experienced successfully for some mixed oxide compounds.[16,17] The Pechini process is based on the polymeric precursors originated from a polyesterification reaction between the desired metallic citrate and a polyalcohol, usually ethylene glycol. The polymeric precursor method has the advantage of using common reagents and not requiring special atmosphere, and moreover, no aging effects have been reported so far. To the authors' knowledge, no polymeric precursor solutions have been reported for production of Bi-layer structured compounds, so much the worse for SBN. In a previous work,[18] the authors reported the synthesis of SBN phase (powder and thin film) using the polymeric precursor method. SBN phase formation was observed around 650 °C. During the crystallization process, an intermediate fluorite phase was detected, similar to the report of Rodriguez *et al.*,[14] for SBT phase.

Zhu *et al.*[7] obtained specular SBT films when they were deposited at lower temperature and annealed at higher temperature for grain growth. This procedure allowed a homogeneous nucleation at lower temperature and a subsequent densification at higher temperature. The two-step deposition process resulted in dense, homogeneous films with less surface roughness and improved ferroelectric properties.

In this work, the influence of the crystallization route on surface morphology, microstructure, and crystallinity of SBN thin films prepared by the polymeric precursors method is discussed.

II. EXPERIMENTAL PROCEDURES

A. SBN deposition solution

Strontium carbonate, $SrCO_3$ (Merck), niobium ammonium oxalate, $NH_4H_2[NbO–(C_2O_4)_3]\cdot 3H_2O$ (CBMM, Araxá, Brazil), and bismuth oxide, Bi_2O_3 (Aldrich), were

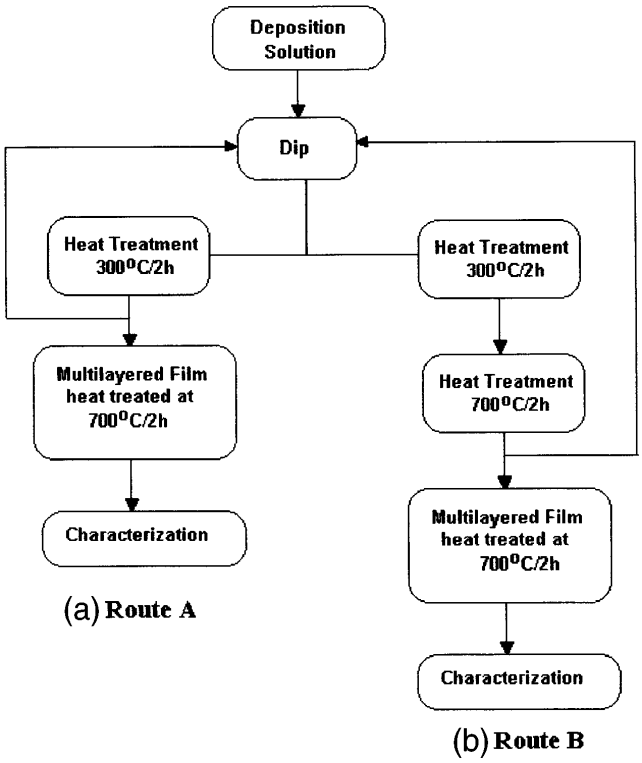

FIG. 1. Procedure for preparation of intermediate-amorphous and intermediate-crystallized layer of multilayered films.

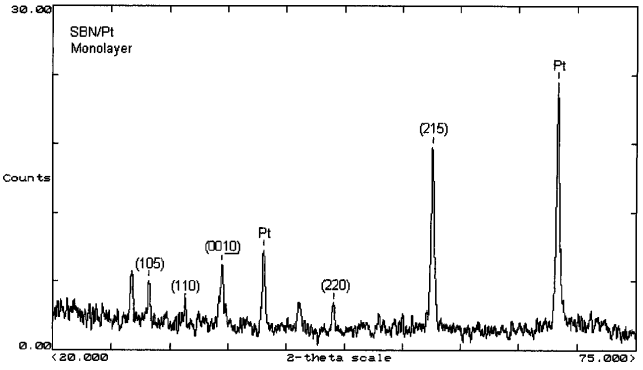

FIG. 2. GIXRD pattern of monolayered SBN film deposited onto Pt.

used as reagents to synthesize $SrBi_2Nb_2O_9$ (SBN). Niobium hydroxide was formed by dissolution of the niobium ammonium oxalate in water and precipitated as $Nb(OH)_5$ by addition of NH_4OH. After filtration, niobium hydroxide was dissolved in an aqueous solution of citric acid to form niobium citrate. The content of Nb was gravimetrically determined as Nb_2O_5. To this niobium citrate solution were added stoichiometric amounts of $SrCO_3$ as salt and Bi_2O_3 dissolved in water with HNO_3. Ethylenediamine was added dropwise into the solution with constant stirring until the pH reached 7–8. After homogenization of the solution,

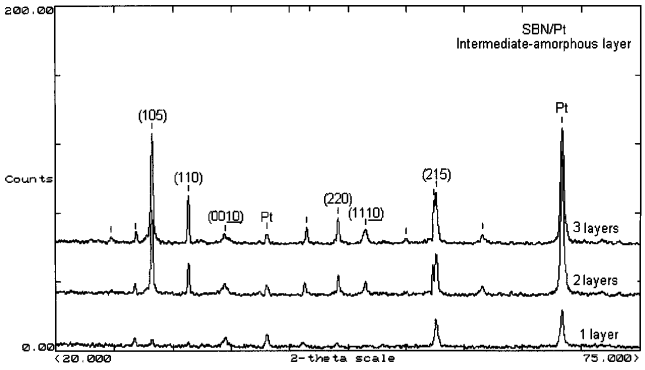

FIG. 3. GIXRD patterns for multilayered SBN films heat-treated at 700 °C with intermediate-amorphous layer.

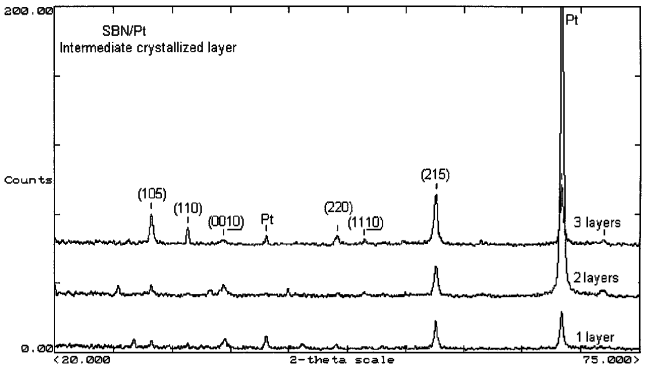

FIG. 4. GIXRD patterns for multilayered SBN films heat-treated at 700 °C with intermediate-crystallized layer.

ethylene glycol was added to promote polymerization of mixed citrate by polyestherification reaction. The molar ratio among strontium, bismuth, and niobium was 1 : 2 : 2, the citric acid/metal molar ratio was fixed at 3.95, and the citric acid/ethylene glycol ratio was fixed as 60/40 (mass ratio). The viscosity of the deposition solution was adjusted by water evaporation until reaching 15 mPa s.

B. Preparation of SBN films

Films were dip-coated from SBN deposition solution onto $Pt/Ti/SiO_2/Si$ substrate. From a previous paper,[18] SBN films were completely crystallized at 700 °C, so this was the temperature at which films were heat-treated. Multilayered films were obtained by dipping two or three times in the deposition solution.

Two sets of multilayered films were heat-treated by two different routes. Route A, films were heat-treated at 300 °C for 2 h and dipped again, until the desired number of layers was reached. Each layer was amorphous and all layers were crystallized at 700 °C for 2 h at the same time. Route B, each layer was heat-treated at 300 °C for 2 h and immediately crystallized at 700 °C for 2 h, before the next one. Hereafter, this

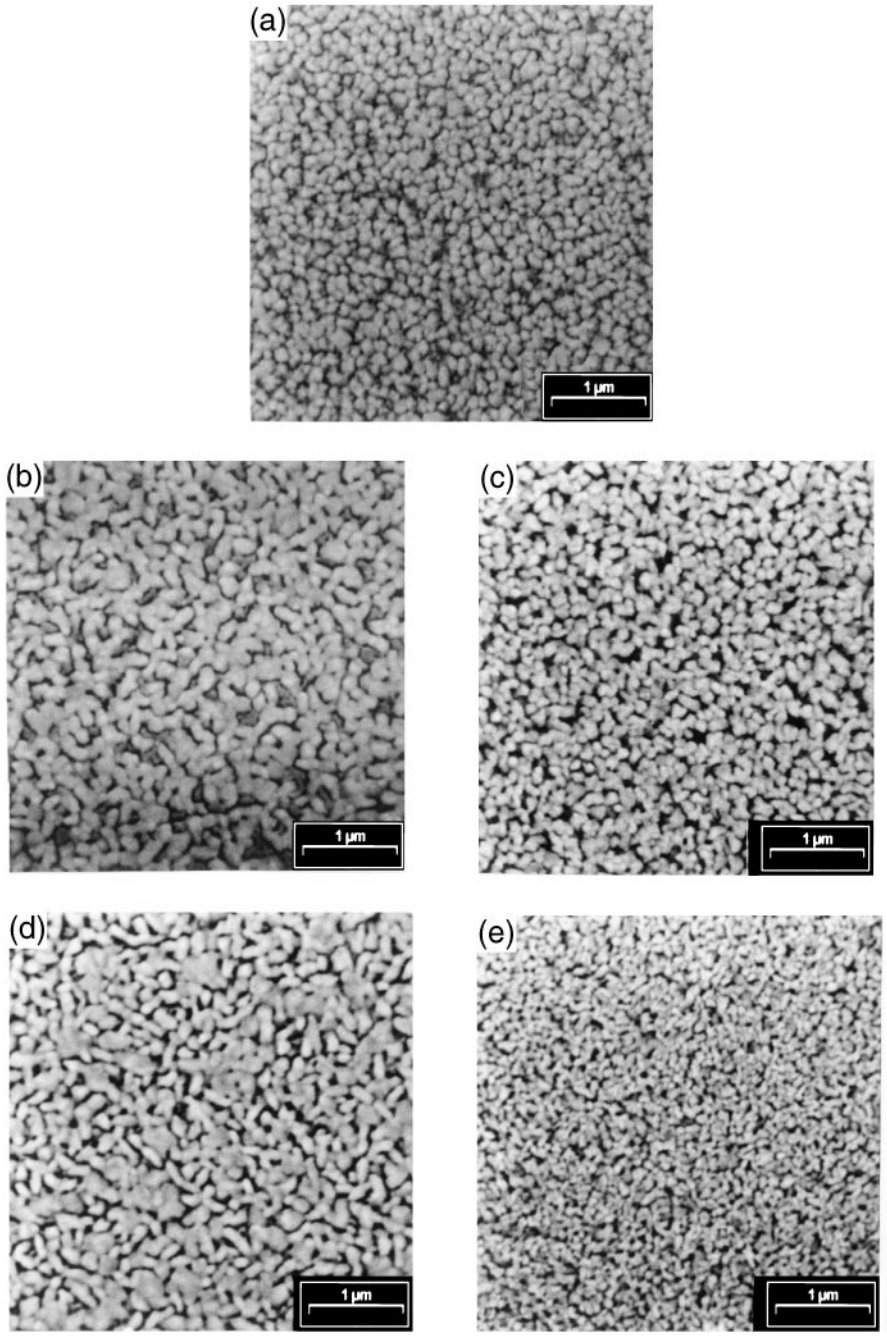

FIG. 5. SEM micrographs of the films heat-treated by both routes: (a) monolayered; double-layered: (b) intermediate-amorphous layer; (c) intermediate-crystallized layer; three-layered: (d) intermediate-amorphous layer; (e) intermediate-crystallized layer.

TABLE I. Evolution of grain size and roughness for multilayered films heat-treated at 700 °C by both routes.

	Grain size (nm)		Roughness/RMS (nm) - 1 μm^2	
Films	Intermediate crystallized	Intermediate amorphous	Intermediate crystallized	Intermediate amorphous
Monolayered	194 ± 25	194 ± 25	2.0	2.0
Double-layered	190 ± 27	233 ± 19	3.8 ± 1.0	5.0 ± 0.9
Three-layered	134 ± 7	275 ± 73	6.4 ± 0.1	5.0 ± 0.8

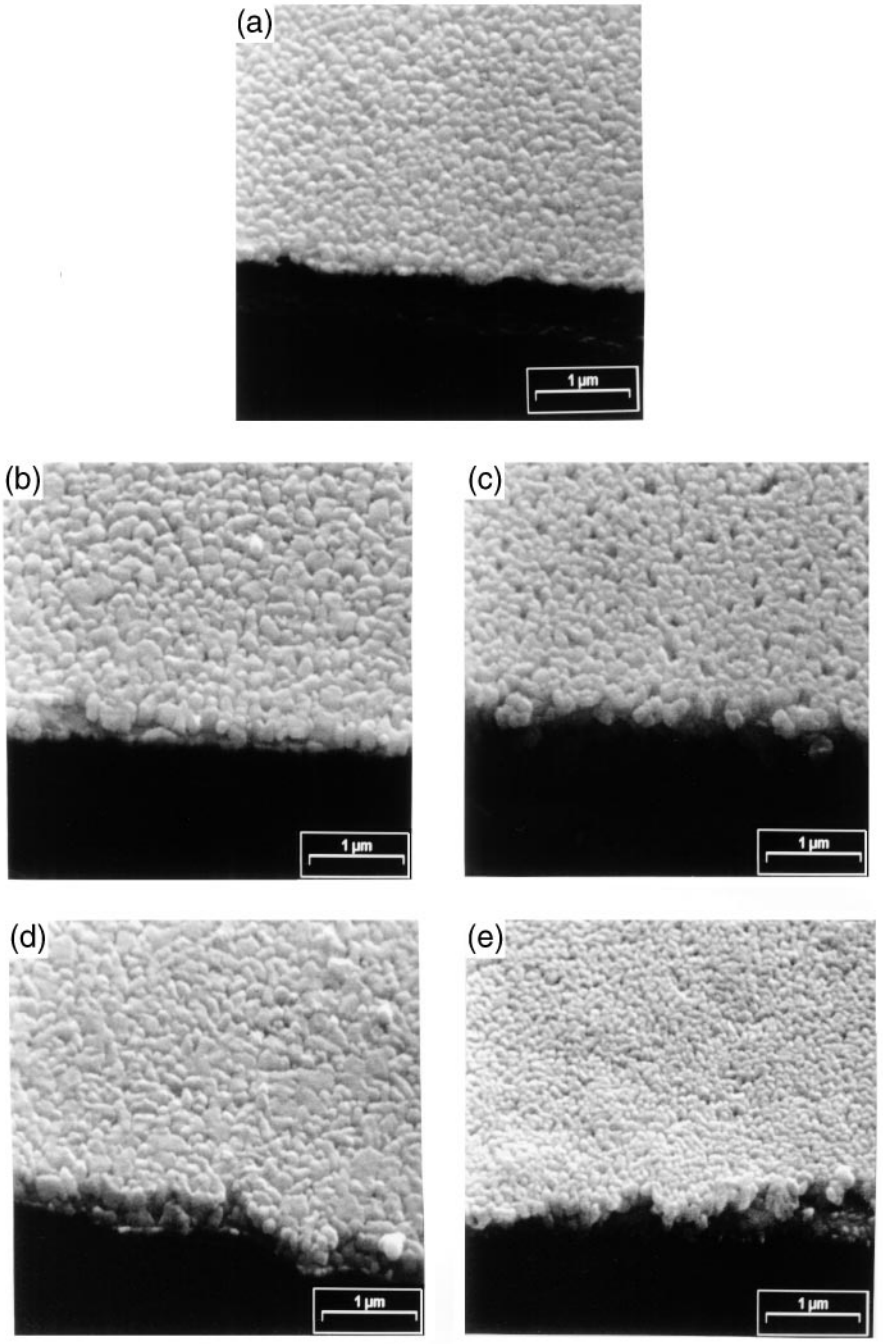

FIG. 6. SEM micrographs of the transversal section of films heat-treated by both routes: (a) monolayered; double-layered: (b) intermediate-amorphous layer; (c) intermediate-crystallized layer; three-layered: (d) intermediate-amorphous layer; (e) intermediate-crystallized layer.

procedure will be called the "intermediate-crystallized layer" route. Figure 1 illustrates the procedure.

Films were characterized by grazing incidence x-ray diffraction (GIXRD) (Siemens, D5000), using an incident angle of 2°(α) and a LiF100 monochromator. Scanning electron microscopy (SEM) (Zeiss, DSM940A), atomic force microscopy (AFM), and scanning tunneling microscopy (STM) (Digital, NanoScope 3A), were used for microstructural characterization. Surface roughness (RMS) was examined by AFM, using tapping mode, and STM.

III. RESULTS AND DISCUSSION

Figure 2 presents the GIXRD pattern of the monolayered film. A SBN perovskite single-phase film with a preferential orientation in the ⟨215⟩ direction can be observed. As the number of layers increases, the

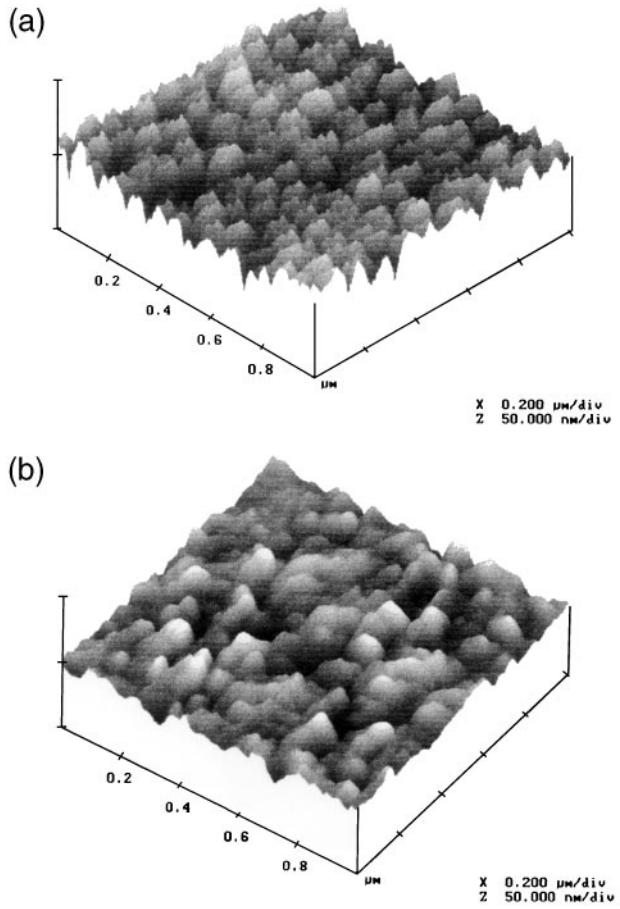

FIG. 7. Morphology of three-layered films heat-treated at 700 °C. (a) Intermediate-crystallized layer; (b) intermediate-amorphous layer.

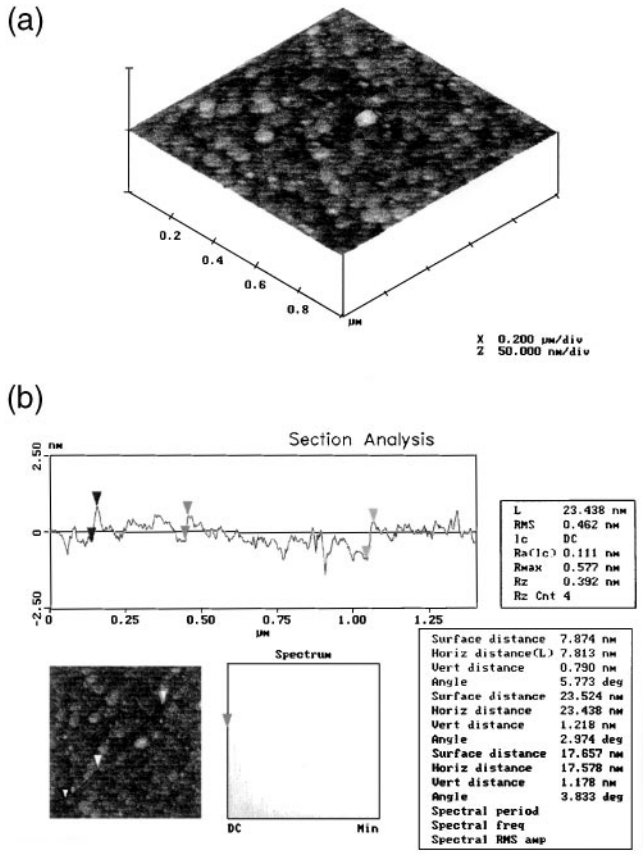

FIG. 8. Morphology of Pt/Si(100) substrate obtained by STM. (a) Surface topography (3D); (b) surface profile.

analysis shall take into account the route B. Figures 3 and 4 illustrate the GIXRD patterns for both routes. As observed for the monolayered film, the multilayered film showed only SBN phase. It can be observed that, for the route A (Fig. 3), x-ray intensity increases as more layers are added, characterizing a polycrystalline film. In contrast, for the route B, films maintain the preferential orientation in the ⟨215⟩ direction, even for three-layered films (Fig. 4). Probably, the thinner layer to be crystallized for route B favors the preferential orientation due to interface nucleation.[19] For route A, the thickness (for two or three layers) may give rise to other phenomena, like surface nucleation, and originates a polycrystalline film as the number of layers is increased.

Figure 5 presents the SEM micrographs of the films heat-treated by both routes. The monolayered film [Fig. 5(a)] presents a dense and granular microstructure, with spherical grains around 194 nm in size. The absence of cracks and fissures indicates that the film presents a homogeneous microstructure. With the different crystallization routes used for multilayered films, a strongly marked difference in the film microstructure can be observed. For the route A [Figs. 5(b) and 5(d)], an increase in the mean size grain is observed as the number of layers is increased. The dense and granular microstructure is maintained, although the grains become elongated (rodlike grains). For route B [Figs. 5(c) and 5(e)], a reduction in mean size grain can be noticed as the number of layers increases (as can be observed in Table I). The multilayered films obtained by the route B maintain a microstructure similar to the monolayered film, a dense and granular structure, with spherical grains.

Figure 6 presents the transversal cross-sectional micrographs of multilayered films by SEM. For both crystallization routes, one can see, clearly, the layers related to the deposition process. After three dips, the film thickness is 235 nm for the route B [Fig. 6(d)] and 258 nm for the route A [Fig. 6(e)].

Figure 7 presents a typical surface morphology of the film heat-treated by both routes. The roughness measured by AFM ranged from 2 to 7 nm. These results are better compared to polycrystalline films obtained by chemical methods[7,11] (ranging from 10 to 43 nm) and similar to that obtained by physical method[20] (nearly 4 nm). Table I presents the average grain size and roughness values for films heat-treated by both routes.

The results presented show that different crystallization routes lead to films with different microstructures. The multilayered films, crystallized using the route A, presented a typical bismuth-layer perovskite structure. As reported for films with good ferroelectric properties, the grain size was around 250 nm with elongated shape.[21,22] On the other hand, the films crystallized using the route B presented spherical grains around 130 nm in size.

Considering both crystallization routes, the route B seems to favor a higher nucleation rate, leading to a higher number of crystalline nuclei. Each intermediate-crystallized SBN layer acts like a nucleation seed to the next layer to be crystallized. Moreover, as can be seen in Table I, the roughness increases as the number of layers increase. This increase in roughness may contribute to the formation of a higher number of sites favorable to the nucleation, which may promote a higher number of crystallization nuclei. As the number of nuclei increases, the grain growth decreases, leading to a fine grain microstructure. Each new layer added conduces to a smaller grain size, mainly due to the increase in the roughness of the previous layer.

In the case of the route A, the nucleation rate may be lower, promoting a lower number of crystallization nuclei, leading to an increase in the grain growth, resulting in a bigger grain microstructure. Basically, the nucleation occurs in the film surface and in the film/substrate interface. The low substrate roughness may contribute to reduce the number of crystallization nuclei. Figure 8 presents a substrate surface morphology, obtained by STM, with roughness around 0.3 nm (RMS).

IV. CONCLUSIONS

It was observed that the crystallization route influences greatly the film microstructure. Multilayered films obtained using the intermediate-crystallized layer route present a dense microstructure with spherical grains. As the number of layers increases, the spherical grain shape is kept, and the mean grain size decreases from 194 to 134 nm, probably due to the increase in each layer roughness. In contrast, multilayered films obtained using the intermediate-amorphous layer route presented elongated grains around 250 nm in size.

The results showed a strong relationship among the substrate roughness, crystallization, and film microstructure.

ACKNOWLEDGMENTS

The authors acknowledge the following Brazilian financing support agencies: FAPESP (Project Nos. 96/9748-0, 96/10118-1), CNPq and CAPES, and CBMM–Cia. Brasileira de Mineração e Metallurgia for supplying the niobium ammonium oxalate.

REFERENCES

1. L. Dat and J. K. Lee, Appl. Phys. Lett. **67**, 572 (1995).
2. J. F. Scott, F. M. Ross, C. A. P. Araujo, M. C. Scott, and M. Huffman, MRS Bull. **21** (7), 33 (1996).
3. H. Tabata, H. Tanaka, and T. Kawai, Jpn. J. Appl. Phys. **34**, 5146 (1995).
4. H-M. Yang, J-S. Luo, and W-T. Lin, J. Mater. Res. **12**, 1145 (1997).
5. O. Auciello, A. R. Krauss, J. Im, D. M. Gruen, E. A. Irene, R. P. H. Chang, and G. E. McGuire, Appl. Phys. Lett. **69** (18), 2671 (1996).
6. N-J. Seong and S-G. Yoon, Appl. Phys. Lett. **71** (1), 81 (1997).
7. Y. Zhu, S. B. Desu, T. Li, S. Ramanathan, and M. Nagata, J. Mater. Res. **12** (13), 783 (1997).
8. T. Li, Y. Zhu, and S. B. Desu, J. Appl. Phys. **68** (5), 616 (1996).
9. Y. Ito, M. Ushikubo, S. Yokoyama, H. Matsunaga, T. Atsuki, T. Yonezawa, and K. Ogi, Jpn. J. Appl. Phys. **35**, 4925 (1996).
10. M. A. Rodriguez, T. J. Boyle, B. A. Hernandez, C. D. Buchheit, and M. O. Eatough, J. Mater. Res. **11**, 2282 (1996).
11. P. Y. Chu, R. E. Jones, Jr., P. Zurcher, D. J. Taylor, B. Jiang, S. J. Gillespie, Y. T. Lii, M. Kottke, P. Fejes, and W. Chen, J. Mater. Res. **11**, 1065 (1996).
12. T. Mihara, H. Yoshimori, H. Watanabe, and C. A. P. Araujo, Jpn. J. Appl. Phys. **34**, 5233 (1995).
13. K. Amanuma, T. Hase, and Y. Miyasaka, Appl. Phys. Lett. **66** (2), 221 (1995).
14. T. J. Boyle, C. D. Buchheit, M. A. Rodriguez, H. N. Al-Shareef, B. A. Hernandez, B. Scott, and J. W. Ziller, J. Mater. Res. **11**, 2274 (1996).
15. M. P. Pechini, U.S. Patent 3,330,697 (1967).
16. S. M. Zanetti, E. R. Leite, E. Longo, and J. A. Varela, Mater. Lett. **31**, 173 (1997).
17. V. Bouquet, E. R. Leite, E. Longo, and J. A. Varela, *Euro Ceramics V–Key Engineering Materials* (Trans. Tech. Publications, 1997), Vols. 132–136, p. 1143.
18. S. M. Zanetti, E. R. Leite, E. Longo, and J. A. Varela, unpublished.
19. C. K. Kwok and S. D. Desu, J. Mater. Res. **8**, 339 (1993).
20. J-K. Lee, H-J. Jung, O. Auciello, and I. Kingon, J. Vac. Sci. Technol. A **14** (3), 900 (1996).
21. T-C. Chen, T. Li, X. Zhang, and S. B. Desu, J. Mater. Res. **12**, 1569 (1997).
22. I. Koiwa, T. Kanehara, J. Mita, T. Iwabuchi, T. Osaka, S. Ono, and M. Maeda, Jpn. J. Appl. Phys. **35**, 4946 (1996).